Kinetic phase transitions in a contaminated monomer-dimer reaction model

V. Bustos, R. O. Uñac, and G. Zgrablich
Laboratorio de Ciencias de Superficies y Medios Porosos, Universidad Nacional de San Luis, Chacabuco 917, 5700 San Luis, Argentina
(Received 15 June 2000)

The irreversible kinetics of a monomer-dimer reaction on a catalyst surface [the Ziff-Gulari-Barshad (ZGB) model] in the presence of a contaminant species is studied by means of Monte Carlo simulation. The only processes allowed to the contaminant are adsorption and desorption; it is otherwise inert. The reaction window, delimited by a second order irreversible phase transition at low monomer concentration (lower bound transition) and by a first order one at high monomer concentration (upper bound transition) in the ZGB model is found to shrink with increasing contaminant concentration in a way that depends on its adsorption-desorption kinetics. Through epidemic analysis, it is also found that the upper bound transition changes from first to second order and that the lower bound transition can also be affected depending on the contaminant adsorption-desorption kinetics. The results may provide alternative explanations for experimental observations.

PACS number(s): 02.70.Lq, 05.70.Ln, 82.20.Mj, 82.65.Jv

I. INTRODUCTION

Recent advances in surface science [1–6] are opening a new trend in research on catalytic reactions, in the sense that they try to bridge the gap between ideal ultrahigh vacuum (UHV) studies of molecular reactions on perfect crystals and the results of catalytic reactions performed under industrial conditions [7]. These conditions introduce three drastic differences with respect to UHV ideal studies: (a) the active solid is not a perfect crystal, (b) the reaction does not occur in UHV but at a pressure many orders of magnitude higher under thermodynamic equilibrium between the gas phase and the adsorbed phase, and (c) the reactants are not pure but contaminated with other species.

Some of the recent developments allow atomic scale monitoring of surface species during catalytic reactions at high pressures on both flat and stepped crystals [1–3], while others deal with adsorption and reaction kinetic studies at high pressure on different surfaces [4–6]. All these research directions reveal behaviors not observed in UHV studies. In the present work we address from a theoretical point of view the effects of the third factor mentioned above, the presence of a contaminating species, on a widely studied reaction: the monomer-dimer (MD) irreversible reaction, inspired by the catalytic oxidation of CO, which presents kinetic phase transitions.

The study of kinetic, or irreversible, phase transitions (IPT's) became popular with the seminal work of Ziff, Gulari, and Barshad [8], who proposed the popular ZGB model, and has continued attracting the attention of researchers ever since [9]. Even if the ZGB model is oversimplified, it has proved to be useful in understanding the main features of a kind of IPT. The outstanding feature of this model is to present a reaction window delimited by a dimer-poisoned state characterized by a second order IPT, at low monomer concentration (lower bound), and by a monomer-poisoned state characterized by a first order IPT, at high monomer concentration (upper bound). The lower bound IPT has been carefully characterized through epidemic analysis [10] as belonging to the directed percolation (DP) universality class [11]. In spite of its amazing simplicity, the ZGB model had great success in the prediction of a reaction window observed in one of the most studied monomer-dimer catalyzed reactions, CO oxidation on transition metals. In fact, this reaction window is simply the consequence of spatial correlations induced by a delicate site-particle stoichiometric balance: the monomer (CO) needs one single empty site to adsorb while the dimer (O_2) needs two. The presence of the contaminant, in the present study, will somewhat disturb such balance and therefore it is expected that some important changes in the behavior of the kinetics should appear.

Experimental studies of CO oxidation on transition metals, like, for example, the one given in Ref. [12], present, however, two mainly differences with respect to the predictions of the ZGB model.

(i) The lower bound second order DP transition to an oxygen-poisoned state has not been found. The reaction rate rather increases steadily as CO concentration increases from zero, passes through a maximum, and then becomes stationary at a very low value. Several reasons can be invoked to explain this discrepancy, like the possible contribution of the Eley-Rideal mechanism to the reaction [13–15], the influence of quenched disorder softening the transition [11], and the experimental difficulty of maintaining a perfect nonfluctuating oxygen-poisoned state.

(ii) The upper bound first order transition is rather seen as a second order one. Several effects have been shown to produce this result: CO desorption [16], a fractal substrate [17], and lateral interactions [18,19].

The results we are going to present here suggest possible alternative explanations for these observed differences.

The work is organized as follows. In Sec. II the model and simulation method are described. Results for the kinetic phase diagrams are presented and discussed in Sec. III. Section IV is dedicated to studying the characteristics of the lower and upper bound IPT's through epidemic analysis, and conclusions are given in Sec. V.

II. MODEL AND SIMULATION METHOD

The reaction model we propose here is a very simple modification of the ZGB model to study the effects of a

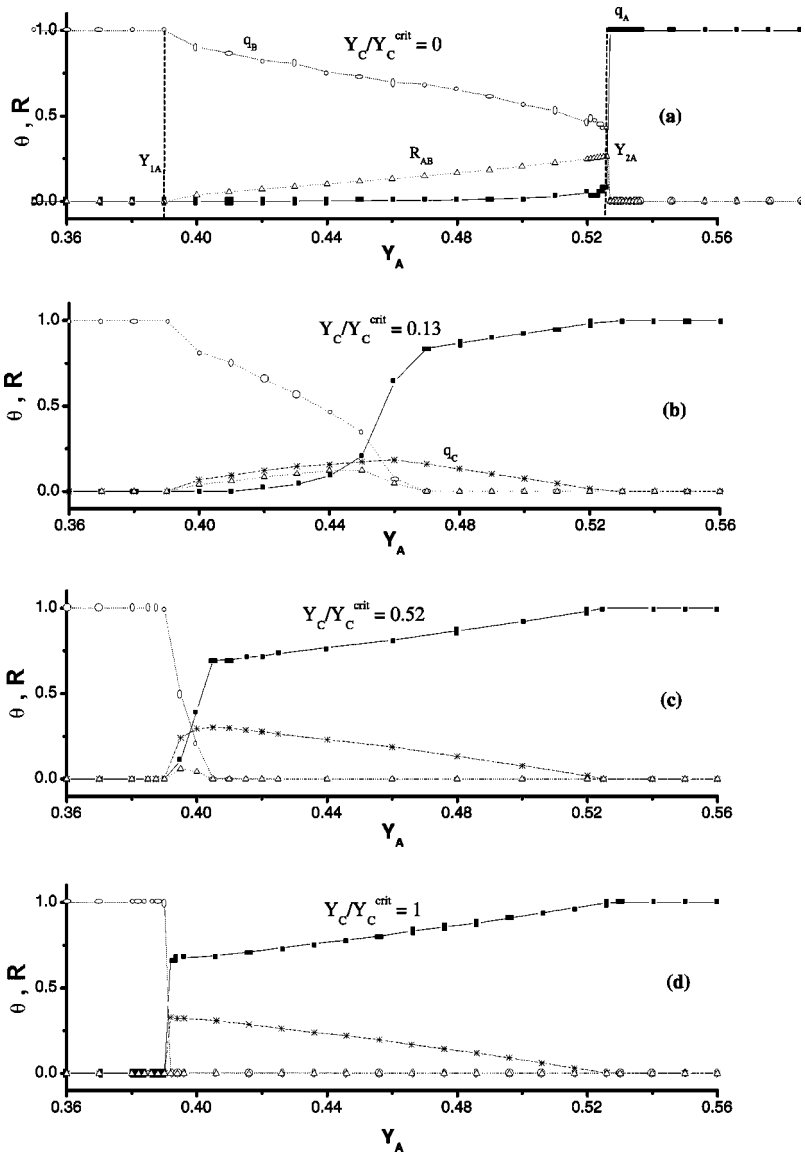

FIG. 1. Steady state mean coverage and reaction rate for the contaminated monomer-dimer reaction, for different contaminant concentrations increasing from (a) to (d), under kinetics *A*. ■, *A* coverage; ○, *B* coverage; ∗, *C* coverage; △, *AB* reaction rate.

monomer contaminant species on the MD reaction. Let *A* be the monomer, B_2 the dimer, and *C* the contaminant. We propose the following reaction steps:

$$A(\text{gas}) + \text{site} \xrightarrow{Y_A} A(\text{ads}), \tag{1}$$

$$B_2(\text{gas}) + 2 \text{ sites} \xrightarrow{1-Y_A} 2B(\text{ads}), \tag{2}$$

$$C(\text{gas}) + \text{site} \overset{k_{a,d}(Y_C)}{\leftrightarrow} C(\text{ads}), \tag{3}$$

$$A(\text{ads}) + B(\text{ads}) \xrightarrow{\infty} AB(\text{gas}) + 2 \text{ sites}. \tag{4}$$

In the CO oxidation reaction, for example, *A* is CO, B_2 is O_2, *AB* is CO_2, and *C* could be any impurity in the reactant gases, for example, N_2. In the above reaction system the contaminant species *C* undergoes only adsorption-desorption processes, being otherwise inert. Our model is a two-parameter one, say, Y_A and Y_C. We study two different kinetics for species *C*.

Kinetics *A*

For the adsorption and desorption rates we take, respectively,

$$k_a = Y_C(1-\theta), \quad k_d = Y_C(1-\theta)\theta_C, \tag{5}$$

where θ is the total surface coverage and θ_X is the coverage for species *X*. This kinetics, if *C* were the only species present, would lead to complete saturation of the surface.

Kinetics *B*

A different kinetics, leading to saturation in surface coverage of species *C* below the monolayer if *C* were the only species present, could be the following:

$$k_a = Y_C(1-\theta), \quad k_d = Y_C\theta_C. \tag{6}$$

As we shall see, even very small amounts of contaminant, such as those present in realistic reaction conditions, drastically affect the reaction kinetics and the position and characteristics of the IPT's.

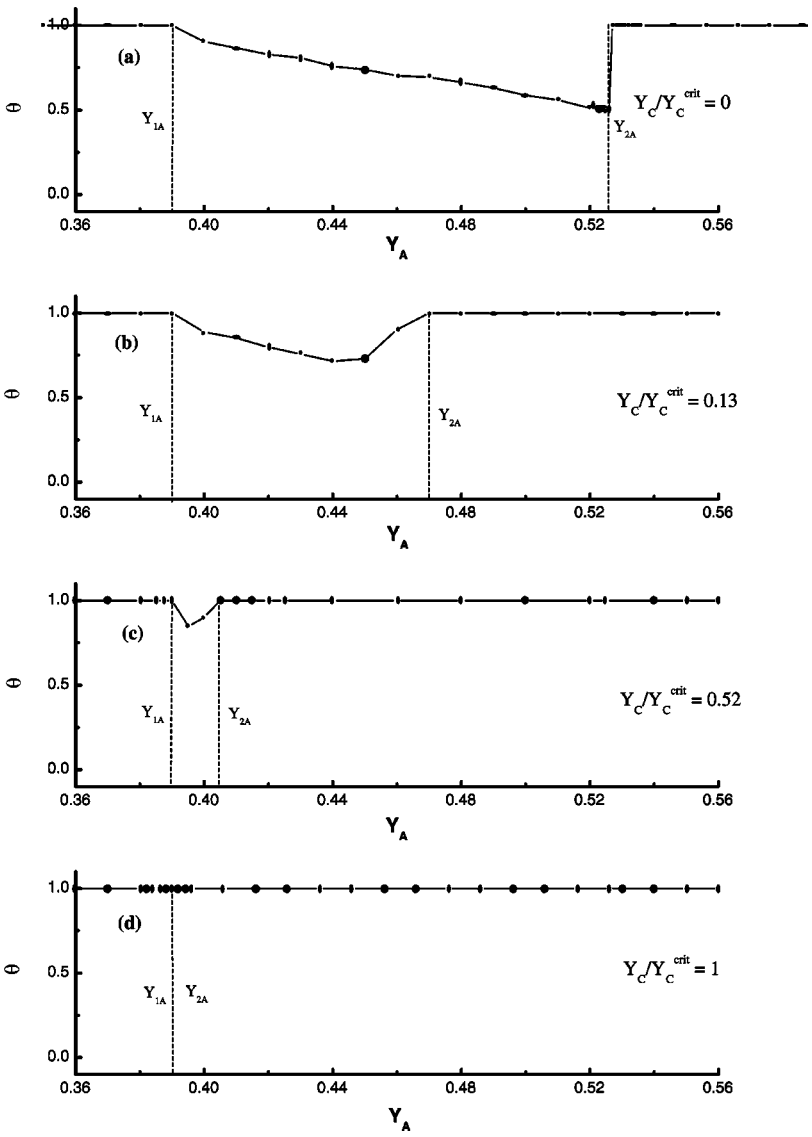

FIG. 2. Steady state total mean coverage (●) for kinetics *A*, showing the shrinking of the reaction window as the contaminant concentration increases from (a) to (d).

We study the behavior of the proposed system through Monte Carlo simulation by following closely the method used in the original ZGB model [8] with the obvious modifications imposed by step (3). The catalyst surface is represented by a square lattice of sites, with dimensions $L \times L$ ($L = 100$ in our simulations) and periodic boundary conditions. The gas phase is represented by a mixture of the three reactant species with mole fractions Y_A, Y_B, and Y_C, such that they sum up to unity.

A trial begins by choosing a species from the gas phase with probabilities given by the respective mole fractions.

If the chosen molecule is A, then (a) a site on the lattice is chosen at random; (b) if that site is already occupied, then the trial ends; (c) otherwise *A* is adsorbed; and (d) the four nearest neighbor (NN) sites are checked in random order. If a *B* is found in any of them, then both sites are emptied and a reaction product *AB* is accumulated.

If the chosen molecule is B_2, then (a) two adjacent sites are chosen at random; (b) if either site is occupied, the trial ends; (c) otherwise B_2 dissociates and adsorbs on those two sites; and (d) the six NN sites are checked in random order. If an *A* is found in any of them, then it is reacted with the adjacent *B*, both sites are emptied, and a reaction product *AB* is accumulated.

If the chosen molecule is C, then there are two possibilities. *For kinetics A* (a) a site on the lattice is chosen at random; (b) if it is occupied, then the trial ends; (c) otherwise *C* is adsorbed; and (d) another site in the lattice is randomly chosen; (e) if it is *C*, then it is desorbed, otherwise the trial ends. *For kinetics B* (a) a site on the lattice is chosen at random; (b) if it is empty, *C* is adsorbed; or (c) if it is a *C*, then it is desorbed; (d) otherwise the trial ends.

A Monte Carlo step (MCS) consists of $L \times L$ trials, i.e., in the mean every site on the lattice has been visited for adsorption. For given values of Y_A and Y_C, and starting with an initial blank state, stabilization of the process is achieved either when the total surface coverage $\theta = \theta_A + \theta_B + \theta_C$ is unity or when it has not changed appreciably over the last 10^5 MCS's. In all cases stabilization is achieved before 70×10^5 MCS's. In this way a plot of each species coverage and of the reaction rate R_{AB} versus Y_A is obtained for each value of Y_C.

III. KINETIC PHASE DIAGRAMS

We present and discuss our results for each of the kinetics considered for the contaminant species.

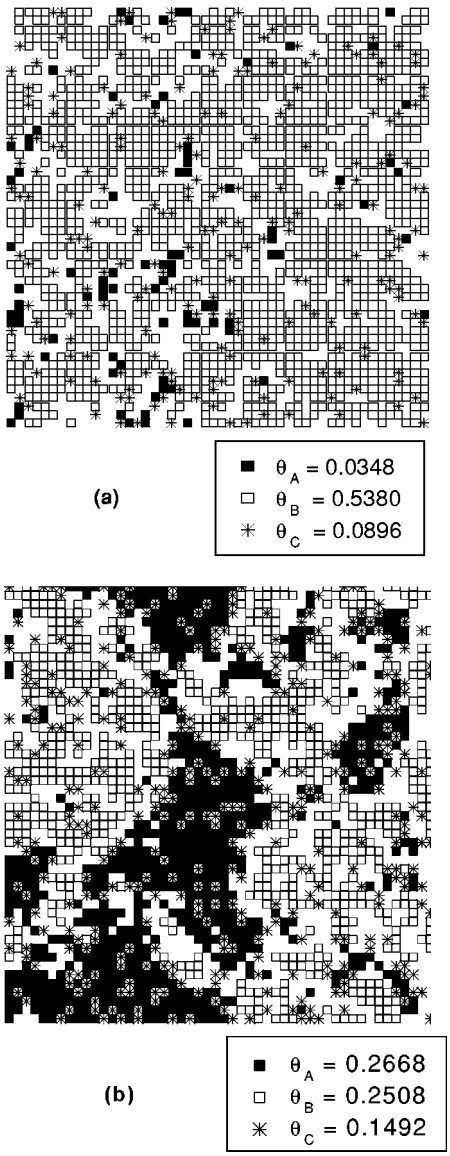

FIG. 3. Monte Carlo snapshots of surface coverage for $Y_A = 0.47$ and $Y_C = 1 \times 10^{-7}$, for kinetics *A*: (a) after 30×10^5 MCS's; (b) after 50×10^5 MCS's.

Kinetics *A*

As shown in Fig. 1, the behavior of the steady state coverage and that of the reaction rate as a function of Y_A are strongly affected by the contaminant concentration. In (a), for $Y_C = 0$, we have the classical ZGB behavior with a second order IPT at $Y_{1A} = 0.389 \pm 0.005$ (for $Y_A < Y_{1A}$ there is a *B*-poisoned state) and a first order IPT at $Y_{2A} = 0.525 \pm 0.001$ (for $Y_A > Y_{2A}$ there is an *A*-poisoned state) and the reaction window between these two values. As Y_C increases [(b) and (c)], the low Y_A IPT remains unchanged, with the only exception that near Y_{1A} a few *C* particles also contribute to the *B*-poisoned state, while the high Y_A IPT becomes smoother and continuously moves to the left until the reaction window completely disappears in (d), when the contaminant concentration reaches a critical value $Y_C^{\text{crit}} \approx 7.5 \times 10^{-7}$ for the assumed kinetics. The behavior of the reaction window can be better appreciated in Fig. 2, where only the total surface coverage has been represented as a function of Y_A. The reaction window (broken lines), delimited by a (*B* $+C$)-poisoned state at the lower bound, and by an $(A+C)$-poisoned state at the upper bound [20], shrinks continuously down to zero.

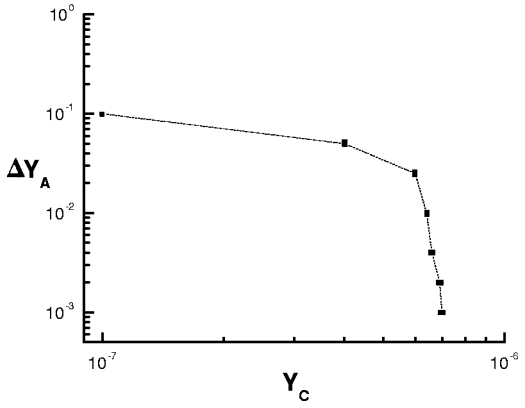

FIG. 4. Variation of the size of the reaction window as a function of the contaminant concentration, for kinetics *A*.

In order to analyze these results we must recall that, as is well known from the ZGB model, the *A*-poisoned state is achieved through an abrupt growth of compact *A* islands (a condensation process) when criticality is approached. When Y_A is not sufficiently high, adsorption of the dimer B_2 and the eventual reaction prevent the explosive growth of islands and the reaction is sustained. Let us see what happens near Y_{1A} [for example, $Y_A = 0.47$ in Figs. 1(b) and 2(b), corresponding to $Y_C / Y_C^{\text{crit}} = 0.13$] when the contaminant *C* is present. At an intermediate stage in the stabilization process, where $\theta_A = 0.0348$, $\theta_B = 0.5380$, and $\theta_C = 0.089$ [see snapshot in Fig. 3(a)], the contaminant in the adsorbed phase is in part dispersed among a sea of *B* and empty sites while another fraction is in contact with small *A* islands. The former have negligible effect on the process since the adsorption of the monomer *A* on empty sites next to *B* is still highly probable. In contrast, those *C* in contact with small *A* islands partially prevent the breaking down of the islands by adsorption of the dimer, through a decrease in the adsorption probability of a dimer in their surroundings (two sites are needed). In a sense, we could say that *C* favors the nucle-

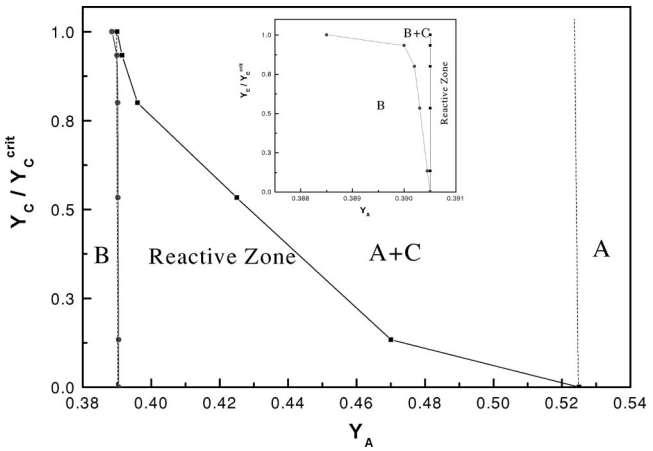

FIG. 5. Phase diagram for the contaminated monomer-dimer reaction, for kinetics *A*, showing the different poisoned regions and the reaction region. The inset shows an enlargement near the lower bound of the reaction window.

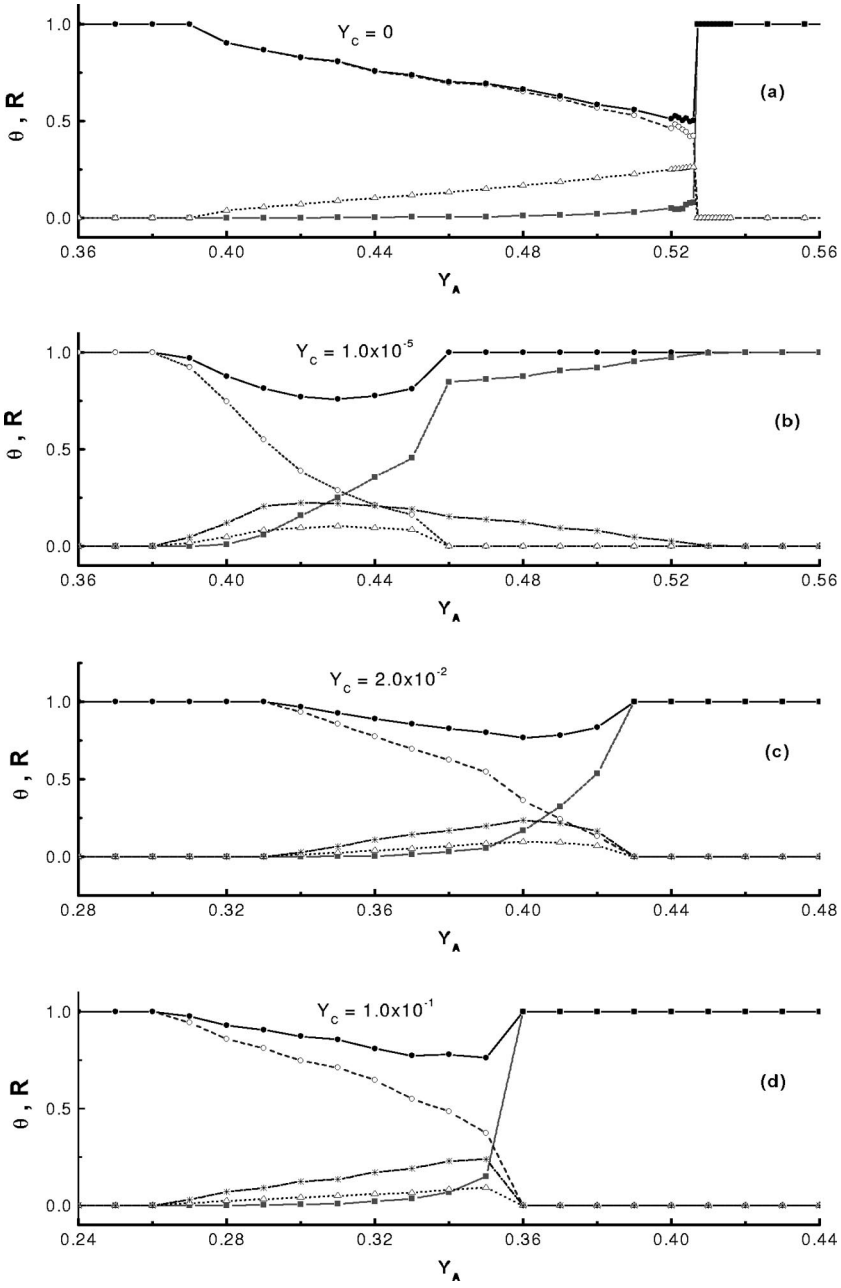

FIG. 6. Steady state mean coverage and reaction rate for the contaminated monomer-dimer reaction, for different contaminant concentrations increasing from (a) to (d), under kinetics *B*. ■, *A* coverage; ○, *B* coverage; ∗, *C* coverage; ●, total coverage; △, *AB* reaction rate.

ation and growth of these islands. As the process goes on, at a stage where $\theta_A=0.2668$, $\theta_B=0.2508$, and $\theta_C=0.1492$ [see snapshot in Fig. 3(c)], *A* islands are much bigger, with an appreciable amount of *C* trapped inside and another fraction in contact with their borders, while the situation in the sea of *B* and empty sites is similar to that corresponding to the previous stage. All this results in a multiple island nucleation, growth, and coalescence process leading continuously to the *A*-poisoned state, with some *C* embedded inside, ending up with coverages given by $\theta_A=0.8424$, $\theta_B=0$, and $\theta_C=0.1576$. The overall effect of the contaminant is then to make the reaction process near the upper bound appear as that corresponding to a higher effective *A* concentration. This explains why the reaction window shrinks, by shifting the upper bound to the left while the lower bound remains unaffected.

The form in which the reaction window ΔY_A shrinks as a function of Y_C is represented in Fig. 4. In the neighborhood of Y_C^{crit}, where the window disappears, ΔY_A behaves as $\Delta Y_A \propto (Y_C^{\mathrm{crit}}-Y_C)^{\zeta}$, with $\zeta=2.83\pm0.23$, giving a critical value of $Y_C^{\mathrm{crit}}=(7.5\pm0.2)\times10^{-7}$. Figure 5 shows the phase diagram for the reaction considered, with the *B*-poisoned, the $(B+C)$-poisoned (in the inset), the reactive, the $(A+C)$-poisoned, and the *A*-poisoned zones.

For the kinetics considered, we conclude that very small amounts (vestiges) of contaminants lead to drastic changes in the reaction process and to the disappearance of the reaction window.

Kinetic *B*

While for kinetics *A* only the upper bound IPT is affected, for kinetics *B* we find that both transitions are. From Fig. 6 we see that the presence of the contaminant again smooths the upper bound IPT, but now it modifies not only the position of the upper bound IPT but also that of the lower bound

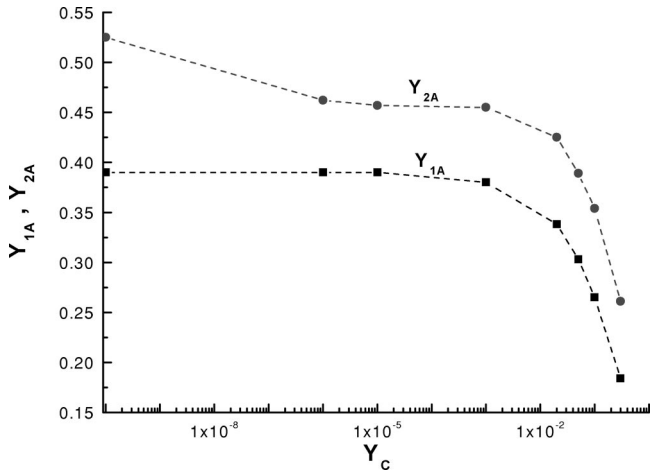

FIG. 7. Position of the upper (●) and lower (■) bounds of the reaction window for kinetics *B* as a function of contaminant concentration.

IPT. For low enough Y_C, say below 1×10^{-5}, the lower bound stays constant while the upper bound shifts to the left. As Y_C increases further, both bounds shift to the left and for high contaminant concentrations the lower bound shifts faster than the upper bound (see Fig. 7). This results in the variation of the width of the reaction window shown in Fig. 8, where it is seen that the reaction window decreases initially, passes through a minimum around $Y_C=1\times10^{-5}$, and then increases again slowly.

The shift in the upper bound can be analyzed by following closely the arguments used in the case of kinetics *A*, with the obvious difference that the shift is much smoother due to the characteristics of kinetics *B*. If the contaminant concentration were increased far beyond the value shown in Figs. 7 and 8, the reaction window would eventually close due to an abrupt shift of the upper bound to the left.

It is interesting to note that the lower bound of the reaction window seems to decrease with no limit toward $Y_A=0$ as the contaminant concentration increases. In fact, this should be so, given that the particular kinetics considered for *C* is such that adsorbed *C* can always be removed, providing free sites for the adsorption of *A* to react with *B* and sustaining the reaction even at low *A* concentrations for sufficiently high Y_C. This behavior provides an alternative explanation for the fact that an oxygen-poisoned state is not found in the CO oxidation reaction [12].

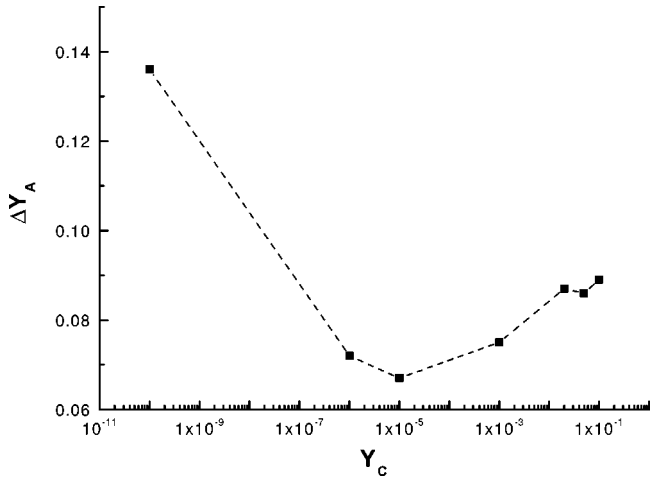

FIG. 8. Variation of the size of the reaction window as a function of the contaminant concentration, for kinetics *B*.

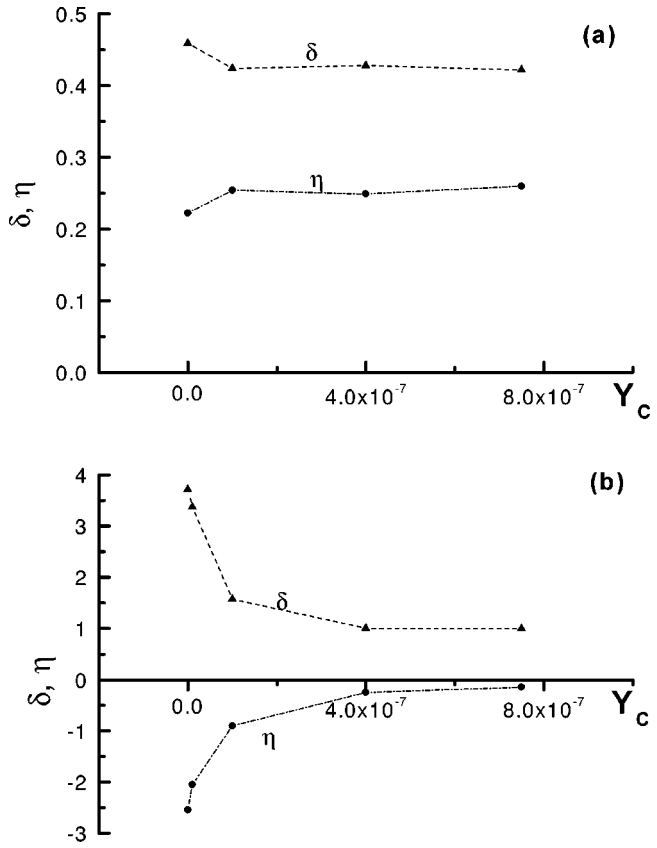

FIG. 9. Critical exponents δ and η as a function of the contaminant concentration, for kinetics *A*: (a) at the lower bound of the reaction window the IPT is second order with constant exponents and nearly belongs to the DP universality class; (b), at the upper bound the IPT is first order at zero contaminant concentration and changes to second order as the concentration increases.

IV. THE NATURE OF THE PHASE TRANSITIONS

Finally, we investigate the nature of the phase transitions at the lower and upper bounds delimiting the reaction window. In order to avoid the large fluctuation problems arising near criticality [9], we make use of the epidemic analysis due to Jensen, Fogedby, and Dickman [10] and the method of

TABLE I. Values of the critical exponents δ and η near the lower and upper bound IPT's for kinetics *A*.

	Y_C				
	0	1×10^{-8}	1×10^{-7}	4×10^{-7}	7.5×10^{-7}
			Lower bound		
η	+0.22		+0.25	+0.25	+0.26
δ	+0.46		+0.42	+0.43	+0.42
			Upper bound		
η	−2.54	−1.69	−0.90	−0.25	−0.14
δ	+3.71	+3.35	+1.57	+1.01	+1.00

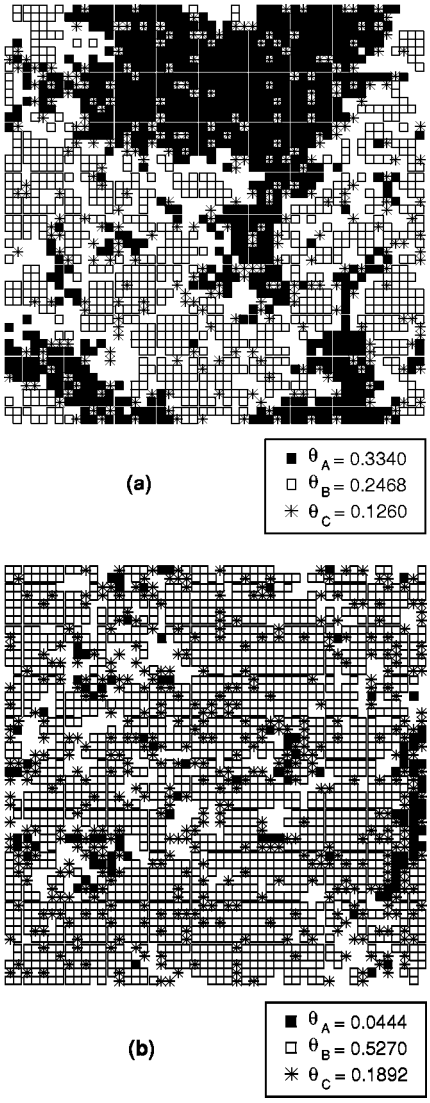

FIG. 10. Monte Carlo snapshots of surface coverage after 2.5×10^5 MCS's: (a) $Y_A=0.48$, $Y_C=0.975\times10^{-7}$; (b) $Y_A=0.405$, $Y_C=3.9\times10^{-7}$.

Evans and Miesch [21,22] to estimate critical exponents. At the lower bound, we start with a lattice completely covered with species B except for a single empty site at its center. Then we measure the survival probability $P(t)$, i.e., the probability that the lattice is not completely poisoned after time t, and the average number of empty sites $N(t)$. These quantities, before they reach their asymptotic behavior, should scale as

$$P(t)\propto t^{-\delta}, \tag{7}$$

$$N(t)\propto t^{\eta}. \tag{8}$$

A unit of time is represented by 1 MCS following the trial procedure described in Sec. II and for each time the measured quantities were averaged over 5×10^3 realizations of the process. A similar analysis is performed at the upper bound, except that we start with a pair of nearest neighbor empty sites embedded in a lattice covered by species A. The results depend on the kinetics considered for the contaminant species.

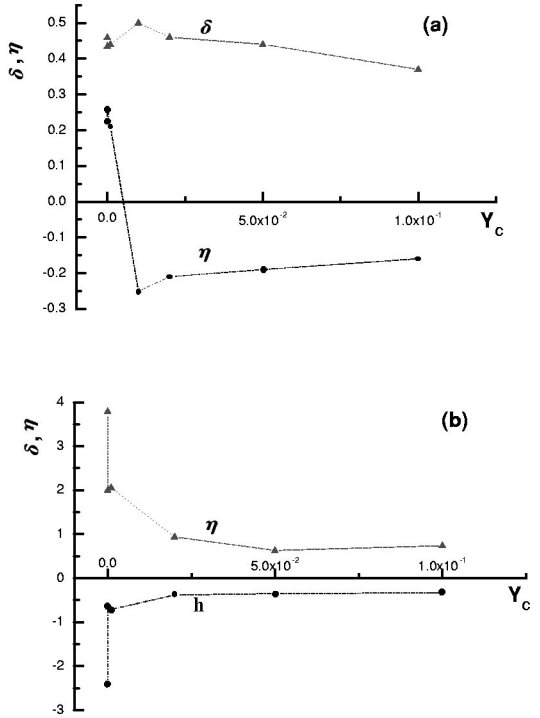

FIG. 11. Critical exponents δ and η as functions of the contaminant concentration, for kinetics B: (a) at the lower bound of the reaction window the IPT is second order, not belonging to the DP universality class; (b) at the upper bound the IPT is first order at zero contaminant concentration and changes to second order as the concentration increases.

Kinetics *A*

The behavior of the critical exponents δ and η at the lower bound IPT are shown in Fig. 9(a) for different values of Y_C. They appear to be nearly independent of the contaminant concentration and their values are close to those obtained by Jensen, Fogedby, and Dickman [10] for the pure ZGB model (see also Table I) corresponding to a second order IPT belonging to the directed percolation universality class. In our case we could say that the DP universality is nearly conserved. This is not an unusual result since it is possible that uncorrelated spatiotemporal quenched disorder, like that introduced in the system by the presence of C under kinetics A, may not disturb the DP critical behavior on large scales [11].

For the upper bound IPT, estimations of the critical exponents as functions of Y_C are shown in Fig. 9(b). Here we find a drastic change in the characteristics of the IPT: for $Y_C=0$, the pure ZGB model, the results are in concordance with those obtained by Evans and Miesch [21,22] and characterize a first order IPT; as Y_C increases, δ decreases while η increases (becomes less negative) until they become nearly stationary. It is interesting to note that critical directed percolation processes can be generated by using properly correlated initial conditions, in such a way that the time behavior of the empty site density may present a critical exponent η ranging from negative to positive values [23]. However, the connection of this observation with our results is not clear. On the other hand, Evans and Miesch [21,22] find that near the upper bound IPT for the ZGB model the exponent δ decreases and the exponent η increases (becomes less negative) when

TABLE II. Values of the critical exponents δ and η near the lower and upper bound IPT's for kinetics *B*.

	Y_C						
	0	1×10^{-5}	1×10^{-3}	1×10^{-2}	2×10^{-2}	5×10^{-7}	1×10^{-1}
				Lower bound			
η	+0.22	+0.26	+0.21	−0.25	−0.21	−0.19	−0.16
δ	+0.46	+0.43	+0.44	+0.50	+0.46	+0.44	+0.37
				Upper bound			
η	−2.41	−0.62	−0.71	−0.38	−0.35	−0.33	
δ	+3.79	+2.00	+2.06	+0.94	+0.63	+0.74	

the reaction rate is decreased from ∞ to a finite value. Therefore, following their analysis, we can conclude that the variation of the critical exponents obtained in Fig. 9(b) is due to the fact that the presence of the contaminant species decreases the effective reaction rate through the same topological mechanism affecting the growth of *A* islands explained in Sec. III. In particular, we find that the IPT at this upper bound has changed from first order (for $Y_C=0$) to second order (for $Y_C>0$); however, this second order transition is determined, through the analysis of critical exponents, not to be in the directed percolation universality class. This change in the order of the phase transition is in concordance with our observation that in the contaminated case the monomer-poisoned state is reached through a continuous process of nucleation, growth, and coalescence of islands, rather than through an explosive growth of a compact island (condensation) as happens in the original ZGB model. Snapshots of the adsorbed phase for $Y_C=0.8\times10^{-7}$ (where critical exponents vary strongly) and for $Y_C=4.0\times10^{-7}$ (where they level out), for values of Y_A just above the IPT and after the same number of MCS's (2.5×10^5), are shown in Figs. 10(a) and 10(b), respectively. A big *A* cluster can be observed in (a), while in (b) we only have a number of small islands, suggesting that in the first case the process looks more like a first order transition while in the second case it looks more like a second order one.

Kinetics *B*

Figure 11 and Table II show the behavior of critical exponents δ and η as a function of Y_C for the case of kinetics *B*. At the lower bound [Fig. 11(a)], while δ remains approximately constant (near the value corresponding to the DP universality class), η decreases initially very fast and then stabilizes to a negative value. This indicates that the dimer-poisoning process no longer belongs to the DP universality class in spite of the fact that it is still a second order IPT. Therefore, we have here an example of a spatiotemporal quenched disorder affecting the universality of the DP process at criticality. At the upper bound [Fig. 11(b)], the critical exponents behave in a similar way to the case of kinetics *A*: δ decreases and η increases with Y_C. The explanation is similar to that given for the case of kinetics *A* (a decrease in the effective reaction rate).

V. CONCLUSIONS

In summary, we have examined the changes in the kinetics of a monomer-dimer catalyzed reaction, represented by the ZGB model, produced by the presence of vestiges of a contaminant species in the gas phase, which only undergoes adsorption-desorption processes, being otherwise inert. A rich variety of behaviors in the reaction kinetics is found, depending on the kinetics assumed for the adsorption-desorption process of the contaminant species (kinetics *A* and *B*).

In all cases, the first order IPT predicted by the ZGB model at high monomer concentration is transformed into a second order IPT, which does not belong to the DP universality class. This finding provides an alternative explanation for one of the features observed experimentally in the CO oxidation reaction (the upper bound IPT is second order).

For kinetics *A*, the second order IPT at the lower bound is not affected by the contaminant and is found to belong nearly to the DP universality class, the upper bound IPT shifts to the left, and the reaction window shrinks and disappears completely at a critical contaminant concentration. For kinetics *B*, the positions of both IPT's are affected by the contaminant in such a way that the reaction window initially shrinks, passes through a minimum, and then widens slightly. The lower bound second order IPT is found not to belong to the DP universality class and continuously shifts toward very low monomer concentrations. This behavior provides an alternative explanation for another feature observed experimentally in the CO oxidation reaction (there is no oxygen-poisoned state).

ACKNOWLEDGMENTS

This research was partially supported by the Consejo Nacional de Investigaciones Científicas y Técnicas (CONICET) of Argentina. The authors would also like to thank their colleague V. Pereyra for helpful discussions.

[1] X. C. Su, P. S. Cremer, Y. R. Shen, and G. A. Somorjai, Phys. Rev. Lett. **77**, 3858 (1996).

[2] J. A. Jensen, K. B. Rider, M. Salmeron, and G. A. Somorjai, Phys. Rev. Lett. **80**, 1228 (1998).

[3] G. A. Somorjai and G. Rupprechter, J. Phys. Chem. B **103**, 1623 (1999).

[4] M. Kaltchev, D. Stacchiola, H. Molero, G. Wu, A. Blumenfeld, and W. T. Tysoe, Catal. Lett. **60**, 11 (1999).

[5] D. Stacchiola, H. Molero, and W. T. Tysoe, Catal. Today (to be published).
[6] S. Azad, M. Kaltchev, D. Stacchiola, G. Wu, and W. T. Tysoe, J. Phys. Chem. B (to be published).
[7] B. J. McIntyre, M. Salmeron, and G. A. Somorjai, Rev. Sci. Instrum. **64**, 687 (1993).
[8] R. M. Ziff, E. Gulari, and Y. Barshad, Phys. Rev. Lett. **56**, 2553 (1986).
[9] For a comprehensive review, see E. V. Albano, Heterog. Chem. Rev. **3**, 389 (1996). For some more recent developments, see also J. Cortés and E. Valencia, Surf. Sci. **245**, L357 (1999).
[10] I. Jensen, H. C. Fogedby, and R. Dickman, Phys. Rev. A **41**, 3411 (1990).
[11] H. Hinrichsen, Ann. Phys. (Leipzig) (to be published).
[12] M. Ehasi, M. Matloch, O. Frank, J. H. Block, K. Christmann, F. S. Rys, and W. Hirschwald, J. Chem. Phys. **91**, 4949 (1989).
[13] J. Mai and W. Von Niessen, Chem. Phys. **156**, 63 (1991).
[14] P. Meakin, J. Chem. Phys. **93**, 2903 (1990).
[15] B. Zhang and H. Y. Pan, J. Phys. A **27**, L651 (1994).
[16] E. V. Albano, Appl. Phys. A: Solids Surf. **55**, 226 (1992).
[17] E. V. Albano, Surf. Sci. **235**, 351 (1990).
[18] H. P. Kaukonen and R. M. Nieminen, J. Chem. Phys. **91**, 4380 (1989).
[19] J. J. Luque, F. Jiménez-Morales, and M. C. Lemos, J. Chem. Phys. **96**, 8535 (1992).
[20] In some cases the upper bound poisoned state may also contain some few *B* completely surrounded by *C* sites.
[21] J. W. Evans and M. S. Miesch, Surf. Sci. **245**, 401 (1991).
[22] J. W. Evans and M. S. Miesch, Phys. Rev. Lett. **66**, 833 (1991).
[23] H. Hinrichsen and G. Odor, Phys. Rev. E **58**, 311 (1998).